NUMERICAL ASSESSMENT OF REDUCED ORDER MODELING TECHNIQUES FOR DYNAMIC ANALYSIS OF JOINTED STRUCTURES WITH CONTACT NONLINEARITIES

Jie Yuan*, Fadi El-Haddad, Loic Salles
Department of Mechanical Engineering
Imperial College London
SW7 2AZ, London, UK
Email: jie.yuan@Imperial.ac.uk
f.el-haddad@imperial.ac.uk
l.salles@imperial.ac.uk

Chian Wong
Rolls-Royce plc
PO Box 31, DE24 8BJ, Derby, UK
Email: Chian.Wong@Rolls-Royce.com

ABSTRACT

This work presents an assessment of classical and state of the art reduced order modelling (ROM) techniques to enhance the computational efficiency for dynamic analysis of jointed structures with local contact nonlinearities. These ROM methods include classical free interface method (Rubin method, MacNeal method), fixed interface method (Craig-Bampton), Dual Craig-Bampton (DCB) method and also recently developed joint interface mode (JIM) and trial vector derivative (TVD) approaches. A finite element jointed beam model is considered as the test case taking into account two different setups: one with a linearized spring joint and the other with a nonlinear macroslip contact friction joint. Using these ROM techniques, the accuracy of dynamic behaviors and their computational expense are compared separately. We also studied the effect of excitation levels, joint region size and number of modes on the performance of these ROM methods.

NOMENCLATURE

n	Number of harmonic numbers
m	Number of DOFs in system
m_j	Specific numbers of harmonics
$f^{(i)}$	Continuation parameter
$f^{(i+1,0)}$	Predicted continuation parameter
g_b^1, g_b^2	Boundary force vector
q	Modal coordinates
$\boldsymbol{A_1}, \boldsymbol{A_2}$	Signed Boolean localization matrix corresponding to 1st and 2nd substructure
$\boldsymbol{B_T^1}, \boldsymbol{B_T^2}, \boldsymbol{B_N^1}, \boldsymbol{B_N^2}$	Boolean matrix of DOFs in tangential direction (T) and normal direction (N) corresponding to the 1st and 2nd substructure separately
$\boldsymbol{B_T}, \boldsymbol{B_N}$	Boolean matrix of DOFs in tangential direction and normal direction on the contact interface
$D_{\tilde{u}}, D_f$	Partial derivatives of the residual to unknowns and frequency
F_{ex}^1, F_{ex}^2	External forces of 1st and 2nd substructure
F_T, F_N	Nonlinear tangential and normal forces
F_{nl}	Nonlinear force vector
$\boldsymbol{G_1}, \boldsymbol{G_2}$	Flexible residuals
$\boldsymbol{I}$	Identity matrix
R	Residual in the Newton method
$\boldsymbol{M_1}, \boldsymbol{M_2}$	Mass matrix of substructures
$\boldsymbol{M}, \boldsymbol{K}$	Global mass and stiffness matrix
N_0	Pre-loading in the joint
$\boldsymbol{K_1}, \boldsymbol{K_2}$	Stiffness matrix of substructures
$\boldsymbol{K_{joint}}$	Linear stiffness matrix of the joint
$\boldsymbol{T}$	Transformation matrix
ω	Fundamental excitation frequency
η_1, η_2	Modal participation factors
μ	Friction coefficient
u_b^1, u_b^2	Physical boundary DOFs
$\tilde{u}_o$	Zero harmonic frequency response
u^1, u^2	Physical displacement
$\tilde{u}_j^c, \tilde{u}_j^s$	Sine and cosine harmonic coefficient at j^{th} harmonic number
$\boldsymbol{\varphi_1^{JIM}}, \boldsymbol{\varphi_2^{JIM}}$	Joint interface mode vector
$\boldsymbol{\varphi_1^{TVD}}, \boldsymbol{\varphi_2^{TVD}}$	Trial vector derivative vector
$\boldsymbol{\phi_1^{fix}}, \boldsymbol{\phi_2^{fix}}$	Fixed interface modal displacements
$\boldsymbol{\varphi_1}, \boldsymbol{\varphi_2}$	Constrain modes
$\boldsymbol{\varphi_{i,j}}$	Derivative of i^{th} linear mode to j^{th} modal displacement
$\boldsymbol{\phi_1^{free}}$ $\boldsymbol{\phi_2^{free}}$	Free interface modes
$\boldsymbol{\phi_{1,b}}$	Free interface modes corresponding to the interface DOFs
$\frac{dF_T}{d\Delta x}, \frac{dF_T}{d\Delta y}, \frac{dF_N}{d\Delta x}, \frac{dF_N}{d\Delta y}$	Derivatives of tangential friction and normal contact force
$\Delta x, \Delta y$	Tangential and normal relative displacement
Δx_c	Relative tangential sliding position
Δs	Step length in continuation

ABBREVIATIONS

iDFT	Inverse discrete Fourier transform
AFT	Alternating frequency time

CB	Craig-Bampton
CBI	Craig-Bampton with interface reduction
CMS	Component mode synthesis
DCB	Dual Craig-Bampton method
DOF	Degree of Freedom
FE	Finite Element
FRF	Frequency response function
JIM	Joint interface modes
MHB	Multi-Harmonic balanced
MAC	Modal assurance criteria
NF	Natural frequency
ROM	Reduced order modelling
RR	Reduction ratio
POD	Proper orthogonal decomposition
TVD	Trial vector derivatives

INTRODUCTION

Mechanical joints are always existing in an assembly when single components are integrated into a more complex structure [1]. They are particularly effective to hold together a structure and transfer the loads from one structural element to another [2, 3]. However, the joint in an assembly significantly augments and complicates the static and dynamic behaviours because of its internal contact friction nonlinearities e.g. the change of stability, the jump phenomenon and energy localization [4]. For bolted jointed structures, the contact friction phenomenon can lead to a reduction in the global stiffness due to the relative slipping motion on the contact interface. The damping from the joint due to interface frictional effects can take up to 90% of the total damping in an assembly [1, 5]. Such significant damping is mainly governed by the preloading and also the friction coefficients of contacting surfaces [2]. As a result, the joints are commonly used as one of the dominant fastening mechanisms for gas turbine assembled structures. For example, bladed disk systems comprise contact interfaces with frictional damper, dovetail joint and other types of nonlinear contact interactions [6, 7]. They can effectively mitigate the high cycle fatigue problems particularly in bladed disk systems. These critical gas turbine components are usually subjected to high mechanical stress during the service conditions by the thermal loads, static fluid pressure and rotation-induced centrifugal loads [8]. The modal densities of bladed disk can be also very high due to a widely dense range of rotational frequency spectrum [9]. Considering the reliable service life and also efficient design of such an assembly, its dynamical behaviours must be captured accurately and efficiently [1]. However, the finite element (FE) discretization method for analysing such jointed structures is often impeded by the unaffordable computational expense. This is mainly attributed to the inherent nonlinearities within the joint that are characterised by the amplitude dependent stiffness and amplitude dependent damping, and also due to the modal size that commonly involves hundreds of thousands and even millions of DOFs [1]. The time integration method is traditionally used to solve such nonlinear systems, for example, using classical Runge-Kutta method or implicit methods like Newmark approach [10]. In general, these methods can deliver accurate results for transient response but are not computationally feasible for the dynamic analysis of large FE structures because small time steps are always required for capturing the high frequency dynamics on the contact friction interface [10]. Fortunately, from the design perspective, the steady state responses due to the periodic loading are far more important than others. This steady state response of nonlinear system can be alternatively obtained by using the multi-harmonic balance (MHB) approach. The MHB method has already shown its high efficiency for the analysis of nonlinear forced response of the jointed structures with local contact nonlinearities [7]. However, the method would further expand the size of the nonlinear equations by multiplying the chosen number of harmonic coefficients [7]. In spite of the advance in computer science, the simulation of a large assembly with local nonlinearities remains as a challenge. The nonlinearities from mechanical joints are therefore commonly neglected or linearized in the industrial applications for the large scale system [1]. One of viable approaches to include these nonlinearities into a large assembly is to reduce the model size by several orders of magnitudes using reduced order modelling (ROM) techniques [1].

Component mode synthesis (CMS) techniques are widely used for model order reduction in the linear and nonlinear dynamic simulations of a large-scale assembly. These methods retain the physical interface DOFs between the components that is ideal to apply nonlinear contact friction model [11, 12]. For example, free interface based hybrid approach has been applied to the Imperial in-house code FORSE for model order reduction [13]. Another common approach is Craig-Bampton method that employs the fixed interface modes [1]. Both methods suit well for the jointed structures with localized nonlinearities. The principle of such CMS approaches is to represent the linear system using the linear normal modes and the static impulse modes associated with retained interface nodes. The nonlinear contact elements are then integrated through these retained nodes. The main drawback of these approaches is that the size of the model would be proportional to the number of DOFs involved in nonlinearities [8, 11]. The size of nonlinear DOFs can be very large for a model with a bit large size of contact interface. It would also be increased by the fact that fine mesh tends to be used in the region of interfaces for accurately resolving the contact stress field [8]. The increasing size of the reduced order model would obviously slow down the convergence speed. On the other hand, strong nonlinear force would affect the accuracy of CMS based ROM techniques. Without sufficient number of modes, they might be unable to capture the local elastic deformations in the joint [12]. This drawback seems more apparent in the CB method because the fixed interface modes do not include the deformation information on the interface [8]. Free interface based methods generally are better to describe the local behaviour of contact interfaces but some studies show they may suffer from numerical instabilities [14].

In order to address the above-mentioned problems with CMS techniques, two interface reduction methods were proposed to condense static impulse modes to improve the efficiency. Becker and Gaul developed a common interface reduction technique to optimize the interface constrain modes when using the CB approach [15]. The idea is to replace full size of constrain modes by a subset of eigenvectors. They are obtained from the 2nd modal analysis based on the reduced global matrix by using constrained modes from the 1st modal analysis. The method is referred to CBI in this study. Witteveen proposed another approach to reduce the number of nonlinear DOFs by using joint interface modes [16]. The process of generating these JIMs is to firstly statically condense the whole structure to the joint interface DOFs by respecting the Newton's third law on the interface. This lead to a

reduced system that is used for a subsequent modal analysis. The resulting eigenvectors are so called JIMs. The case study by Gaul and Becker has confirmed the JIM method has superior convergence rate over the common interface reduction method [15]. This is because the JIMs would introduce more local flexibility in the interface that allow for a better accurate description of the interface movement [17]. Similarly, Segalman also presented a generalized version of such a approach but not for a joint focused local nonlinearity problem called Milman-Chu modes [18]. Another recent variant to compute the joint modes is based on the modal derivatives that is so-called trial vector derivatives (TVDs) approach [17, 18]. The idea of TVD approach is to enrich the subspace generated by CMS methods by taking into account the difference of such subspaces to that would have been obtained from the full nonlinear system [17]. TVDs are obtained by the first-order Tyler expansion of the CMS generated subspace. Proper orthogonal decomposition (POD) technique is then used to obtain the most influencing TVD vectors. Both of the TVD and JIM are considered in this paper. In addition, POD itself can be also widely referred as an independent ROM method. It can generate a projection basis using a set of snapshots of a full nonlinear system response. The advantage is being this projection basis models the entire structure without the distinction between DOFs involved. The obvious disadvantage is being that the solution of the full nonlinear system have to be computed firstly [19].

The objective of this paper is to perform a numerical assessment of using classical and also state of the art reduced order modelling (ROM) techniques for the nonlinear dynamic analysis of a jointed structure with contact nonlinearities. These ROM methods include classical free interface method (Rubin method, MacNeal), fixed interface method (CB), DCB method and also JIM and TVD approaches. A finite element jointed beam model, one with a linear joint and the other with a nonlinear joint, are considered as two test cases. The paper is organized as follows: the formulation of the benchmark test cases, a jointed structure with local contact nonlinearities, is firstly presented; it is followed a brief presentation of the ROM techniques, namely the Galerkin projection approach and ROM methods; and then 2D macro-slip contact friction model and also the nonlinear MHB solver are introduced; we then introduce the two test case respectively following the discussions of the accuracy and computational cost between these ROM methods.

SYSTEM FORMULATION

A nonlinear system consisting of two connected substructures with local contact friction is considered. Figure 1 illustrates an example of such a system made up of two cantilever 3D beams (Substructure 1 and Substructure 2) and also a contact frictional joint in between which is demonstrated by using 3D macro-slip contact friction element [20]. The nonlinear forces can be expressed as a function of frictional coefficient μ, preloading N_o, contact stiffness k_t, k_n and also the relative displacement on the interface u_b^1, u_b^2. The tangential force is also dependent on the F_N during the slip state. The partial differential governing equation of such a system without taking damping into account can be described as follow:

$$\begin{bmatrix} \boldsymbol{M_1} & \boldsymbol{0} \\ \boldsymbol{0} & \boldsymbol{M_2} \end{bmatrix} \begin{bmatrix} \ddot{u}^1 \\ \ddot{u}^2 \end{bmatrix} + \begin{bmatrix} \boldsymbol{K_1} & \boldsymbol{0} \\ \boldsymbol{0} & \boldsymbol{K_2} \end{bmatrix} \begin{bmatrix} u^1 \\ u^2 \end{bmatrix} = \begin{bmatrix} F_{ex}^1 \\ F_{ex}^2 \end{bmatrix} - \left(\begin{bmatrix} \boldsymbol{B_T^1} \\ \boldsymbol{B_T^2} \end{bmatrix} F_T(u^1, u^2) + \begin{bmatrix} \boldsymbol{B_N^1} \\ \boldsymbol{B_N^2} \end{bmatrix} F_N(u^1, u^2) \right) \quad (1)$$

$$\boldsymbol{M} = \begin{bmatrix} \boldsymbol{M_1} & \boldsymbol{0} \\ \boldsymbol{0} & \boldsymbol{M_2} \end{bmatrix}, \boldsymbol{K} = \begin{bmatrix} \boldsymbol{K_1} & \boldsymbol{0} \\ \boldsymbol{0} & \boldsymbol{K_2} \end{bmatrix}, u = \begin{bmatrix} u^1 \\ u^2 \end{bmatrix} = \begin{bmatrix} u_i^1 \\ u_b^1 \\ u_b^2 \\ u_i^2 \end{bmatrix} \quad (2)$$

$$\boldsymbol{B^1} = \begin{bmatrix} \boldsymbol{B_T^1} \\ \boldsymbol{B_N^1} \end{bmatrix} \quad \boldsymbol{B^2} = \begin{bmatrix} \boldsymbol{B_T^2} \\ \boldsymbol{B_N^2} \end{bmatrix}$$

Where $\boldsymbol{M_1}, \boldsymbol{M_2}, \boldsymbol{K_1}, \boldsymbol{K_2}$ are the mass and stiffness matrix of two substructures; $\boldsymbol{M}, \boldsymbol{K}$ are the global mass and stiffness matrix of linear system; $\boldsymbol{B_T^1}, \boldsymbol{B_T^2}, \boldsymbol{B_N^1}, \boldsymbol{B_N^2}$ are the Boolean matrix related to interface tangential and normal contact DOFs of two substructures where the nonlinear forces are applied; F_{ex}^1, F_{ex}^2 are the external forces on the substructures; F_T, F_N are the nonlinear tangential and normal forces; u^1, u^2 are the displacement of the structure where the subscript *i, b* means the DOFs belong to internal or boundary DOFs.

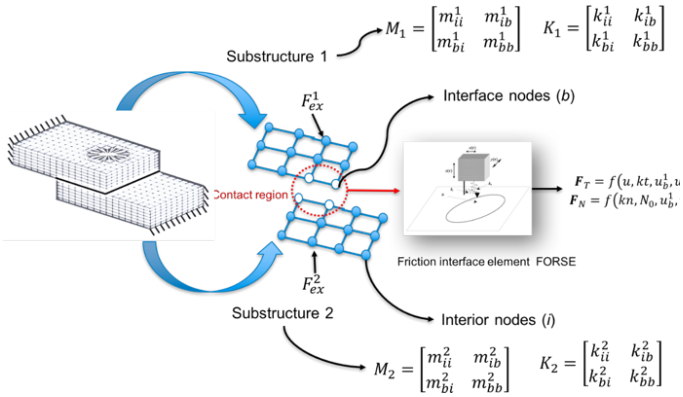

Figure 1. An illustration of a nonlinear jointed structure with contact local nonlinearities

GALERKIN PROJECTION

In the field of structural dynamics, the dynamic response of high dimensional system under the narrow spectrum loading can be approximately condensed in a low dimensional subspace [19]. The solution can be therefore expressed as a linear combination of vectors spanning the subspace, which would significantly reduce the number of unknowns. This type of reduction is generally known as the Galerkin projection. For linear system, this process is well established that uses the corresponding eigenvectors from the linear system as the basis vector which is also called modal superposition. The selection of the reduced basis is crucial in determining the accuracy of the reduced solution. The size of the reduced basis is important to determine the speed-up ratio. Assuming that these vectors form a reduced basis denoted by $\boldsymbol{T}$, the displacement field u can be projected onto the reduced basis as:

$$u(t) \approx \boldsymbol{T}q(t) \text{ where } \boldsymbol{T} = [t_1, t_2 \dots t_m] \quad (3)$$

Where $q(t)$ is the reduced time dependent vector of unknowns and t_i is the i^{th} vector in a reduced basis. Using such a projection, the governing equation (1) becomes:

$$\boldsymbol{T^T M T}\ddot{q} + \boldsymbol{T^T K T}q = \boldsymbol{T^T}F_{ex} - \boldsymbol{T^T}(\boldsymbol{B_T}F_T(\boldsymbol{T}q) \quad (4)$$

$$+\boldsymbol{B_N} F_N(\boldsymbol{Tq}))$$

CRAIG-BAMPTON METHOD

CB method combines normal modes of components obtained by imposing fixed boundary conditions at the interface and static solution (so called constrain modes) for applied boundary displacement at each interface DOF. The global transformation matrix can be seen below:

$$\boldsymbol{T} = \begin{bmatrix} \boldsymbol{\phi_1^{fix}} & \boldsymbol{\varphi_1} & \boldsymbol{0} & \boldsymbol{0} \\ \boldsymbol{0} & \boldsymbol{I} & \boldsymbol{0} & \boldsymbol{0} \\ \boldsymbol{0} & \boldsymbol{0} & \boldsymbol{I} & \boldsymbol{0} \\ \boldsymbol{0} & \boldsymbol{0} & \boldsymbol{\varphi_2} & \boldsymbol{\phi_2^{fix}} \end{bmatrix},$$

$$\begin{bmatrix} u_i^1 \\ u_b^1 \\ u_b^2 \\ u_i^2 \end{bmatrix} = \boldsymbol{T}q = \boldsymbol{T} \begin{bmatrix} \eta_1 \\ u_b^1 \\ u_b^1 \\ \eta_2 \end{bmatrix} \tag{5}$$

Where $\boldsymbol{\phi_1^{fix}}, \boldsymbol{\phi_2^{fix}}$ are the fixed interface modes of the internal coordinates only of two substructures; $\boldsymbol{\varphi_1}$, $\boldsymbol{\varphi_2}$ are the corresponding constrain modes; η_1, η_2 are the modal participation factors; u_b^1, u_b^2 are the displacement vector associated to physical boundary DOFs; $\boldsymbol{I}$ is the identity matrix.

RUBIN METHOD

Rubin method combines free interface normal modes and static ones obtained from the static solution of applied interface load, which is also called attachment modes or flexible residual. The general expression of the transformation matrix without the presence of rigid modes can be described as follows:

$$\boldsymbol{T} = \begin{bmatrix} \boldsymbol{\phi_1^{free}} & \boldsymbol{G_1 A_1^T} & \boldsymbol{0} & \boldsymbol{0} \\ \boldsymbol{0} & \boldsymbol{0} & \boldsymbol{G_2 A_2^T} & \boldsymbol{\phi_2^{free}} \end{bmatrix}$$

$$\begin{bmatrix} u^1 \\ u^2 \end{bmatrix} = \boldsymbol{T} \begin{bmatrix} \eta_1 \\ g_b^1 \\ g_b^2 \\ \eta_2 \end{bmatrix} \tag{6}$$

Where $\boldsymbol{\phi_1^{free}}$ $\boldsymbol{\phi_2^{free}}$ are the free interface modes of these two substructures; $\boldsymbol{G_1}$, $\boldsymbol{G_2}$ are the flexible residuals obtained by the static solution to applied forces on the interface DOFs that the redundant information already included in free modes has been filtered out; g_b^1, g_b^2 are the signed boundary force vectors in the coupled interfaces, which can be transferred back to the boundary displacements using the following matrix as an example for substructure 1:

$$\boldsymbol{T_2^1} = \begin{bmatrix} \boldsymbol{I} & \boldsymbol{0} \\ -\boldsymbol{G_{1,bb}^{-1}} \boldsymbol{\phi_{1,b}} & \boldsymbol{G_{1,bb}^{-1}} \end{bmatrix} \tag{7}$$

Where $\boldsymbol{G_{1,bb}^{-1}}$ is the inversion of the flexible residual matrix related to boundary DOFs; $\boldsymbol{\phi_{1,b}}$ is the free interface modes corresponding to the interface DOFs.

MACNEAL METHOD

The idea of MacNeal method is to simplify the reduced mass matrix by removing the residual inertia term in the transformation matrix as shown below. For the stiffness matrix transformation, it remains same as the Rubin method.

$$\boldsymbol{T_M} = \begin{bmatrix} \boldsymbol{\phi_1^{free}} & \boldsymbol{0} & \boldsymbol{0} & \boldsymbol{0} \\ \boldsymbol{0} & \boldsymbol{0} & \boldsymbol{0} & \boldsymbol{\phi_2^{free}} \end{bmatrix} \tag{8}$$

DUAL CRAIG BAMPTON METHOD

The main idea of the DCB method is to consider the interface connecting forces as unknowns in order to enforce the interface compatibility in a dual assembly fashion. Using the first transformation matrix $\boldsymbol{T}$ in Rubin method, the reduced modal coordinates can be transformed as follows:

$$\boldsymbol{T} = \begin{bmatrix} \boldsymbol{\phi_1^{free}} & \boldsymbol{0} & \boldsymbol{-G_1 B_1^T} \\ \boldsymbol{0} & \boldsymbol{\phi_2^{free}} & \boldsymbol{-G_2 B_2^T} \\ \boldsymbol{0} & \boldsymbol{0} & \boldsymbol{I} \end{bmatrix}, \begin{bmatrix} u^1 \\ u^2 \\ \lambda \end{bmatrix} = \boldsymbol{T} \begin{bmatrix} \eta_1 \\ \eta_2 \\ \lambda \end{bmatrix} \tag{9}$$

Where λ contains the boundary force vector including DOFs on the both sides of the interface, namely g_b^1 and g_b^2. The unknown forces are determined to satisfy the different boundary compatibility conditions. The classical dual assembly is developed only for the case in integrated structures where the absolute displacement on the interface are equal [21]. However, for the coupled structure system with contact friction, force equality with opposite signs is applied to the boundary DOFs instead. In this way, the size of λ can be reduced by half. The linearly coupled system (as shown in the Figure 3) is assembled in a dual fashion as follows:

$$\begin{bmatrix} \boldsymbol{M_1} & \boldsymbol{0} & \boldsymbol{0} \\ \boldsymbol{0} & \boldsymbol{M_2} & \boldsymbol{0} \\ \boldsymbol{0} & \boldsymbol{0} & \boldsymbol{0} \end{bmatrix} \begin{bmatrix} \ddot{u}^1 \\ \ddot{u}^2 \\ \ddot{\lambda} \end{bmatrix} + \begin{bmatrix} \boldsymbol{K_1} & \boldsymbol{0} & \boldsymbol{B_1^T} \\ \boldsymbol{0} & \boldsymbol{K_2} & \boldsymbol{B_2^T} \\ \boldsymbol{B_1} & \boldsymbol{B_2} & \boldsymbol{-K_{joint}^{-1}} \end{bmatrix} \begin{bmatrix} u^1 \\ u^2 \\ \lambda \end{bmatrix} = \begin{bmatrix} F_{ex}^1 \\ F_{ex}^2 \\ 0 \end{bmatrix} \tag{10}$$

Where $\boldsymbol{K_{joint}}$ is the linear stiffness matrix of the joint. The last row of the system describes the linear elastic movement in the joint. For nonlinear joint with contact friction elements, the dual assembled system can be described below.

$$\begin{bmatrix} \boldsymbol{M_1} & \boldsymbol{0} & \boldsymbol{0} \\ \boldsymbol{0} & \boldsymbol{M_2} & \boldsymbol{0} \\ \boldsymbol{0} & \boldsymbol{0} & \boldsymbol{0} \end{bmatrix} \begin{bmatrix} \ddot{u}^1 \\ \ddot{u}^2 \\ \ddot{\lambda} \end{bmatrix} + \begin{bmatrix} \boldsymbol{K_1} & \boldsymbol{0} & \boldsymbol{B_1^T} \\ \boldsymbol{0} & \boldsymbol{K_2} & \boldsymbol{B_2^T} \\ \boldsymbol{0} & \boldsymbol{0} & \boldsymbol{I} \end{bmatrix} \begin{bmatrix} u^1 \\ u^2 \\ \lambda \end{bmatrix} = \begin{bmatrix} F_{ex}^1 \\ F_{ex}^2 \\ F_{nl} \end{bmatrix} \tag{11}$$

Where $\boldsymbol{F_{nl}}$ represents the nonlinear force that would be evaluated by using contact friction model.

JOINT INTERFACE MODES METHOD

The JIM method is to statically condense the system to the joint DOFs by respecting the Newton's third law. Using such a static projection, JIMs can be obtained from the eigen analysis of the resulting reduced mass and stiffness matrix. More details of this process can be referred to [16]. The joint interface modes would employ free interface modes, which is shown as follow:

$$\boldsymbol{T} = \begin{bmatrix} \boldsymbol{\phi_1^{free}} & \boldsymbol{0} & \boldsymbol{\varphi_1^{JIM}} \\ \boldsymbol{0} & \boldsymbol{\phi_2^{free}} & \boldsymbol{\varphi_2^{JIM}} \end{bmatrix}, \begin{bmatrix} u^1 \\ u^2 \end{bmatrix} = T \begin{bmatrix} \eta_1 \\ \eta_2 \\ \eta_{JIM} \end{bmatrix} \tag{12}$$

TRIAL VECTOR DERIVATIVE METHOD

The reduced base vectors of the classical CMS methods are based on the dynamic condensation of linear components, which does not take into account the effect nonlinearities on the linear modes. The idea of the TVD method is to compensate such an effect by including modal sensitivities of the linear reduced basis. The TVDs are defined as a set of the first order derivatives $\boldsymbol{\varphi_{i,j}}$ of each linear base vector $\boldsymbol{\varphi_i}$ to each trial vector weighting factor q_j. They can be approximated by differentiating the eigen equations (where the inertia terms are ignored). The formulation of the TVDs can be then expressed as:

$$\boldsymbol{\varphi_{i,j}} = \boldsymbol{K^{-1}} \frac{\boldsymbol{\partial K}}{\boldsymbol{\partial} q_j} \boldsymbol{\varphi_i} \tag{13}$$

Since the size of TVDs is the square of the size of the CMS base vectors, POD method is used to filter out the redundant information. The detailed derivations can be found in [17]. The TVDs are used with free interface modes. For linear assembled structure shown in Figure 3, we will not consider the gap during the derivation of $\frac{\boldsymbol{\partial K}}{\boldsymbol{\partial} q_j}$. It means the contact stiffness of the joint will be added into $\frac{\boldsymbol{\partial K}}{\boldsymbol{\partial} q_j}$ no matter the normal relative displacement is negative or positive.

$$\boldsymbol{T} = \begin{bmatrix} \boldsymbol{\phi_1^{free}} & \boldsymbol{0} & \boldsymbol{\varphi_1^{TVD}} \\ \boldsymbol{0} & \boldsymbol{\phi_2^{free}} & \boldsymbol{\varphi_2^{TVD}} \end{bmatrix}, \begin{bmatrix} u^1 \\ u^2 \end{bmatrix} = \boldsymbol{T} \begin{bmatrix} \eta_1 \\ \eta_2 \\ \eta_{TVD} \end{bmatrix} \tag{14}$$

CONTACT FRICTION MODEL

A node-to-node approach is used to model the contact friction in the joint [22]. The macro-slip contact law is employed to simulate the contact frictions on the interface, which includes stick, slip and gap states. These states are dependent on the preloading levels and also the amplitude of relative movements on the interface. The 2D macro-slip contact friction model and analytical derivatives of the nonlinear force are written as follows:

$$F_T = \begin{cases} k_t(\Delta x - \Delta x_c) & stick \\ \mu F_N & Slip \\ 0 & Gap \end{cases}$$
$$F_N = \begin{cases} N_0 + k_n \Delta y & stick \\ N_0 + k_n \Delta y & Slip \\ 0 & Gap \end{cases} \tag{15}$$

$$\frac{dF_T}{d\Delta x} = \begin{cases} k_t(1 - \frac{d\Delta x_c}{d\Delta x}) & stick \\ 0 & Slip \\ 0 & Gap \end{cases}$$
$$\frac{dF_T}{d\Delta y} = \begin{cases} 0 & stick \\ \mu k_n & Slip \\ 0 & Gap \end{cases} \tag{16}$$
$$\frac{dF_N}{d\Delta x} = \begin{cases} 0 & stick \\ 0 & Slip \\ 0 & Gap \end{cases}$$
$$\frac{dF_N}{d\Delta y} = \begin{cases} k_n & stick \\ k_n & Slip \\ 0 & Gap \end{cases} \tag{17}$$

Where $(\Delta x, \Delta y)$ are the time-dependent tangential and normal relative displacement within the joint interface; Δx_c is the relative tangential sliding position, which needs to update at each time step; $\frac{\boldsymbol{dF_T}}{\boldsymbol{d\Delta x}}, \frac{\boldsymbol{dF_T}}{\boldsymbol{d\Delta y}}, \frac{\boldsymbol{dF_N}}{\boldsymbol{d\Delta x}}, \frac{\boldsymbol{dF_N}}{\boldsymbol{d\Delta y}}$ are the derivatives of tangential friction and normal contact force in different friction states with respect to the relative displacement. They are used to analytically build the Jacobian matrix which is needed by the Newton-Raphson solver. More details of this modelling approach can be referred to [23, 24].

NONLINEAR SOLVER

The approach used for solving the Eq. (1) in this paper is based on the MHB method. The idea is to represent the steady state non-linear response and also the non-linear forces using truncated Fourier series. The displacement of the nonlinear system is described by n harmonic series:

$$u(t) = \tilde{u}_o + \sum_{j=1}^{n} (\tilde{u}_j^c cosm_j \omega t + \tilde{u}_j^s sinm_j \omega t) \tag{18}$$

Where $\tilde{u}_j^{c,s}$ are cosine and sine harmonic coefficients; n is the number of harmonics; ω is the principal vibration frequency; $\tilde{u}_o$ is the zero harmonic frequency response. With such a representation, the size of whole nonlinear equations is expanded by multiplying the factor of $2n+1$. The Newton-Raphson method, in coupling with the alternating frequency time (AFT) method [25], is used to solve these nonlinear equations. The principle of the AFT technique is to transform the solution from the frequency domain to time domain in order to calculate the nonlinear forces and then transform back using the inverse discrete Fourier transform (iDFT) method. Figure 2 describes the process how this method works with the contact friction model. The initial guess solution can be obtained from the linearized system or using the Homotopy method [26]. The contact friction forces are evaluated by two stages, which is similar to [27]: firstly, the nonlinear contact forces are predicted by assuming the nonlinear force is linearly proportional to relative displacement; the contact forces are then corrected by applying contact friction laws.

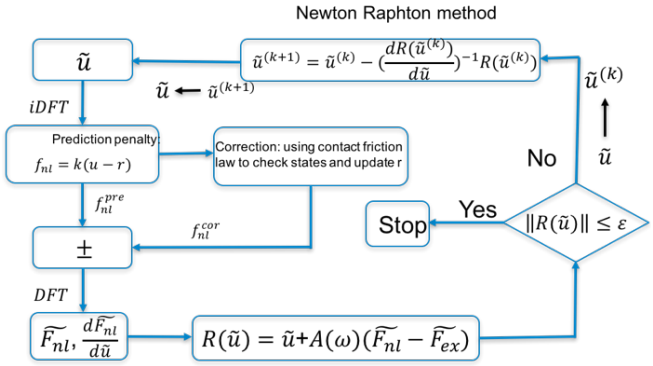

Figure 2 An illustration of Newton-Raphson solver with alternating frequency time scheme

The continuation technique is then used to obtain the forced frequency response of this nonlinear system. The continuation algorithms mainly include two main steps, which are applied sequentially for each frequency point. It is started with a prediction point based on the previous solution followed by the iterative correction steps in order to reach the required tolerance. In this paper, we employ the secant method for the prediction due to its cheap computational cost and arc-length method for the correction step [28]. The secant method uses two previous converged points to obtain the next one as an initial guess as follows:

$$\left(\tilde{u}^{(i+1,0)}, f^{(i+1,0)}\right) = \left(\tilde{u}^{(i)}, f^{(i)}\right) + \Delta s^{i+1}\left(\left(\tilde{u}^{(i)}, f^{(i)}\right) - \left(\tilde{u}^{(i-1)}, f^{(i-1)}\right)\right) \quad (19)$$

Where $f^{(i)}$ is the continuation parameter (namely the frequency) at the previous step and $\tilde{u}^{(i)}$ is the previous convergent solution at $f^{(i)}$; $f^{(i+1,0)}$ is the predicted frequency and $\tilde{u}^{(i+1,0)}$ is the predicted solution at $f^{(i+1,0)}$; Δs^{i+1} is the step length at the $i+1$ step. The objective of the correction step is to move from the predicted point that usually does not satisfy the convergence criteria towards the one does. This is done recursively as follows:

$$\left(\tilde{u}^{(i+1,k+1)}, f^{(i+1,k+1)}\right) = \left(\tilde{u}^{(i+1,k)} + \Delta\tilde{u}, f^{(i+1,k)} + \Delta f\right) \quad (20)$$

$(\Delta\tilde{u}, \Delta f)$ can be the obtained using the linear approximation of residual around the previous iteration solution with imposed Arc length constraints:

$$D_{\tilde{u}}R\left(\tilde{u}^{(i+1,k)}, f^{(i+1,k)}\right)\Delta\tilde{u} + D_f R\left(\tilde{u}^{(i+1,k)}, f^{(i+1,k)}\right)\Delta f + R\left(\tilde{u}^{(i+1,k)}, f^{(i+1,k)}\right) = 0 \quad (21)$$

$$\left\|\tilde{u}^{(i+1,k+1)} - \tilde{u}^{(i)}\right\|^2 + \left|f^{(i+1,k+1)} - f^{(i)}\right|^2 = (\Delta s^{i+1})^2,\ k \gg 0 \quad (22)$$

Where $D_{\tilde{u}}$, D_f are partial derivatives of the residual to unknowns and frequency respectively; $R\left(\tilde{u}^{(i+1,j)}, f^{(i+1,j)}\right)$ is Newton residual at *(i+1)*th step and j^{th} iteration; Eq. (21) is the first order Taylor expansion of the $R\left(\tilde{u}^{(i+1,k+1)}, f^{(i+1,k+1)}\right)$, which include *(2n+1)m* equations. However, *(2n+1) m+1* would be needed for solving the unknowns. This is why Arc length constraint shown in Eq. (22) is imposed on $(\Delta\tilde{u}, \Delta f)$. The adaptive step length Δs based on [26] is applied in order to make the simulation more efficient.

TEST CASE 1-LINEAR JOINTED BEAMS

Figure 3 shows a jointed beam model with linear springs connecting the two equivalent beam substructures. The length of each beam is 0.3m. The width and height of the cross section is 25mm and 6mm respectively. The beam of the substructure is modelled by using the Euler–Bernoulli beam, where each node has three DOFs (u_x, u_y, r_z). The beams are made of steel with a nominal density of 7850 kg/m^3 and Young's modulus of 2.1x10^{11} Nm^{-2}. The tangential stiffness of the springs in the joint is 1x10^4 N/m while normal contact stiffness is 5x10^6 N/m and bending stiffness of 8x10^6 N.m/rad. The total number of nodes is 102, namely 51 nodes for each beam. Figure 4 shows the first nine natural frequencies (NFs) and modes of this linear jointed beam system. These 9 modes all belong to the bending modes. Due to the large value of stiffness in the joint, local elastic modes in the joint did not appear.

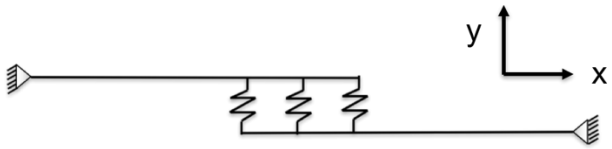

Figure 3 An illustration of the finite element modelling of a jointed beam with springs

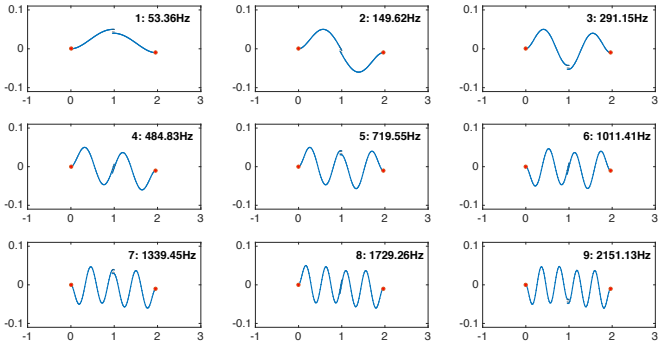

Figure 4 Natural frequencies and mode shapes of linear jointed beam system

Figure 5 shows the variation of NF relative errors with the increasing number of equi-spaced joint nodes (6,18,30 and 42) on the whole beam for each considered ROM method. These ROMs includes global modal superposition (GMS), CB, Rubin, MacNeal, DCB, JIM, TVD. For all the methods, ten normal modes have been used as reduced basis. GMS makes use of global modes of the whole structure including the joint stiffness as the reduced basis. As expected, GMS method results in the smallest errors for a linear system but at the cost of extensive modal analysis of the whole structure. The relative errors from the MacNeal method increase significantly with the size of the joint nodes. It indicates that the residual mass neglected within the MacNeal method has a significant impact on the dynamic of an assembly with the large joint interface. Rubin method overall turns out to be the most accurate one because the free interface modes allow more flexibility on the interface. The relative errors of the first few modes gradually increase 2 to 3 orders while the errors of the high mode (5th to 10th) reduces by 5 orders with the increase of joint nodes on the interface. It is due to the fact that, with the increase of joint nodes, the NFs of the first 10 modes go up and the inertia effect gradually weakens. The static mode in CMS methods therefore has a better approximation for the effects of truncated modes for a stiffer structure. The same phenomenon can be also observed for the Craig-Bampton method but less significant than the Rubin one. In contrast to the Rubin method, CB with the ROM size method has a comparatively poor accuracy that is about 2 to 3 orders less on average. However, CB method appears more numerically robust with the increase of the joint size especially at low number of modes. This is consistent with the literature [8]. JIM approach appears not quite stable and accuracy for the low order modes. The relative errors decrease significantly to 10^{-4} with the number of nodes increases. With the same number of normal modes, it indicates that the JIMs is not good enough to capture the inertia movements that dominates in the low modes. The reformulated DCB method, with the same

size of JIM method, can represent the low order modes very well and even better than the Rubin method. In terms of the accuracy in the high frequency, the reformulated DCB method has the similar relative errors to JIM. TVD method shows very robust performance with the increase of interface nodes, keeping the relative error between 10^{-7} and 10^{-8}. Furthermore, the RR of TVD method is lowest of all the methods. The size of TVD based ROM is independent of the joint interface size. JIM and DCB method has the same reduction ratio. Both of these two methods only retain the half of the interface DOFs.

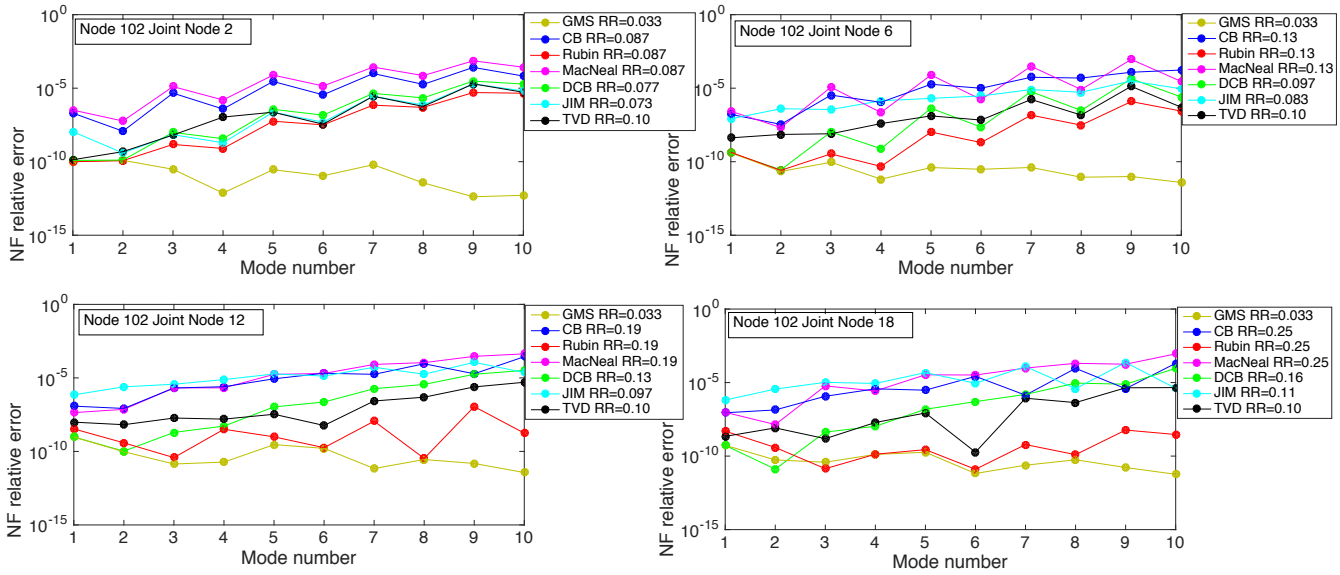

Figure 5 NF relative errors of the jointed beams with increasing number of interface nodes at 6,18,30 and 42 Note: RR stands for reduction ratio (of the number of DOFs)

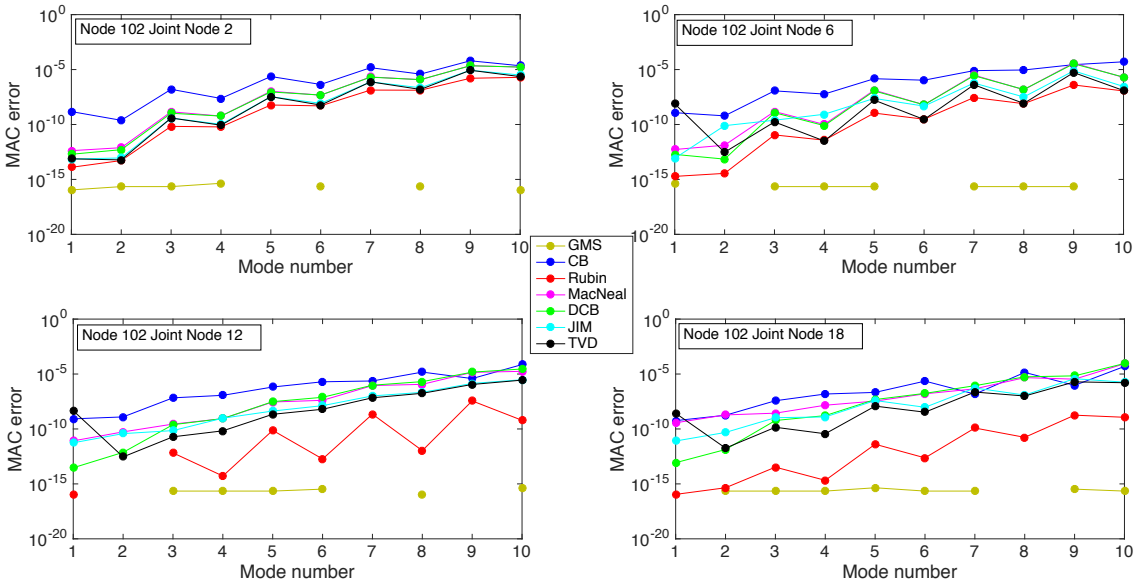

Figure 6 MAC errors of jointed structures with increasing number of jointed nodes

Figure 6 shows the modal assurance criterion (MAC) errors of the eigenvectors computed by these ROMs with the increase of interface node numbers. The MAC is commonly used in experimental measurement to assess the similarity between two mode shape. It is calculated by the normalized scalar product between the two sets of eigenvectors, those value ranges from 0 (unrelated) to 1 (perfect match). More details about MAC can be found in [29]. Herein, one set is chosen from the eigenvector of a full model and the other one chosen from the corresponding reduced order model. The beam configurations are the same as those in Figure 5. It is worth noting that the missing points in yellow and red curves are the ones with MAC value of one. Overall, all of the methods stay low MAC errors under the level of 10^{-5}, except for MacNeal method when the interface node increases to 42. Similar to the conclusions in Figure 5, Rubin method also has the lowest error and its accuracy improve when the number of joint nodes increases, followed by the TVD, JIM and DCB. They cluster together for the most of the first ten

modes. However, for the first two modes, the TVD has a big jump to the level over 10^{-10} while reformulated DCB method keep the lowest MAC errors. CB method again results in large errors in NF errors. However, the errors are very stable with the increase of the interface nodes.

Figure 7 shows the comparison of all the ROM methods with the same size of reduced DOFs. The number of static modes associated to CB, Rubin and MacNeal methods are reduced by half through selecting the odd numbered interface nodes. The result shows the accuracy of CB, Rubin and MacNeal methods are significantly affected with the reduced static modes, making them completely incompetent with the other methods. The CBI method using interface modes instead however has greatly improved the accuracy. The TVD and DCB methods have the smallest NF errors. The DCB method has a better performance than TVD in the first few fundamental modes while TVD is better in the last few modes.

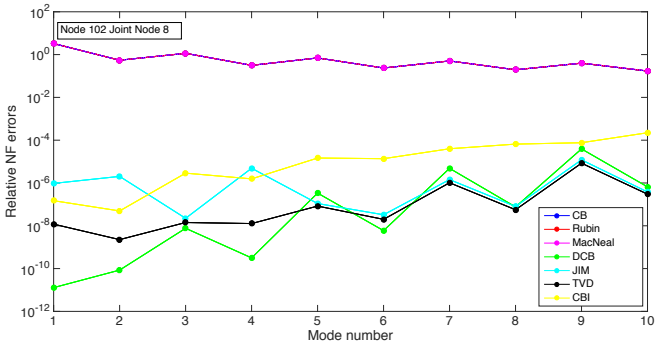

Figure 7 NF relative errors of the jointed beams between the ROMs with the same size

TEST CASE 2-NONLINEAR JOINTED BEAMS

In the case of a nonlinear test case, the joint is modelled by using the 2D contact friction model. The friction model has already been described in Eq. (14-16). Each beam is modelled by using 16 Euler-Bernoulli beam elements. In this case, the tangential friction stiffness in the contact interface is 10^2 N/m while the normal stiffness is 10^4 N/m. The normal preloading in the joint is 20 N and the tangential friction coefficient is 0.3. It is worth noting that the loss of contact is expected to occur during the vibration, because we have not placed torsional spring to simulate the restoring forces in bolted joint. However, we believe the presented case would be sufficient to compare the qualities of different ROM approaches.

Figure 8 shows the modes of a linearized jointed beam with chosen contact stiffness without the torsional spring. The global modes of this assembled structure can be classified into in-phase mode (mode 1,3,5,7 where two structures move in the same direction) and out-of-phase mode (mode 2,4,6,8 where the two structures move in the opposite direction). The NFs of out-of-phase modes are slightly higher than in-phase ones, because the large relative motion in the joint interface further stiffens the jointed structures for out-of-plane modes.

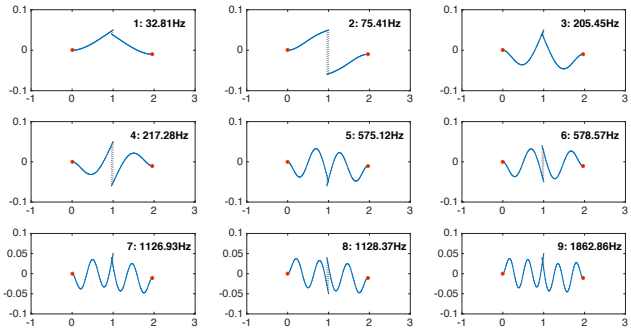

Figure 8 The NFs and modes of a linearized joint beam with contact friction stiffness

Figure 9 shows the frequency response of the nonlinear joint beam close to the first pair of tangential modes at excitation force of 0.1N, 1N, 5N and 10N. Each beam has 16 nodes where the interface between the beams has 2 nodes in this case. The direction of the excitation force and response displacement are both in y direction. As expected, the in-phase mode is on the left with a slightly low resonance frequency while the out-of-phase mode is on the right. We can see that the effect of the nonlinearities on the FRF of the in-plane motion is much less significant due to the small relative elastic deformations in the region of the joint. For the out-of-phase motion on the right, one can observe that the amplitude of the vibration response reduces significantly with the excitation force. At a low excitation level, e.g. 0.1N, the contact interface is in a stuck state when almost no energy is dissipated at the interface. When excitation force level increases, the stuck state cannot maintain anymore, and the macro slip subsequently occurs. The amplitude of the vibration then reduces significantly due to the strong friction energy dissipation as one can observe from the Figure 9.

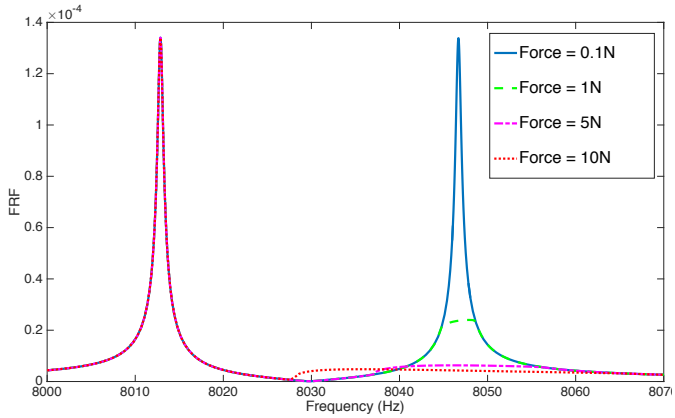

Figure 9 Forced frequency response close to the NFs of the 1st tangential modes under the different excitation levels

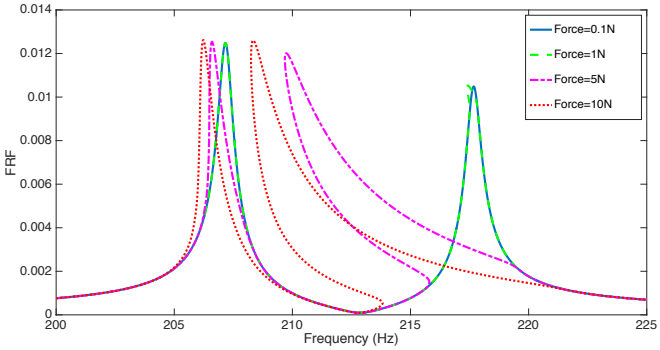

Figure 10 Forced frequency response close to the resonance frequency of the second normal mode pair with the different levels of excitation force

Figure 10 shows the forced frequency function of the nonlinear joint beam close to the frequency of the second pair normal modes with different excitation levels. Similar to the tangential mode in Figure 9, the frequency of the out-of-phase mode is slightly higher. It changes significantly with the increase of excitation levels. The peak of the FRF close to this mode gradually shafts left to the first peak. This means the nonlinearities on the interface have a softening effect, which mainly comes from the gap state activated in joints when the preloading cannot hold the substructures together any more. The separation phenomenon also affects the in-phase mode but has much less.

Figure 11 shows the comparison of the forced frequency response of the beam with four different configurations of interface nodes in the contact region under the same excitation force level of 5 N. With the increase of interface nodes, the resonance frequency of the in-phase mode increases slightly because a large size of contact interface makes the joint structure stiffer and therefore harder to deform. However, the FRF peak of the out-of-phase mode shift more on the left close to the in-phase FRF peak with the increasing size of interface nodes. The resonance frequency of out-of-phase mode increases when the number of joint nodes increases from 2 to 16. The frequency then decreases with the further increase of joint nodes. This indicates that the nonlinear effects become stronger when the number of interface nodes increases. As expected, the peak of the response level is similar with the increase of the interface nodes. This may be due to the decoupled motion between x and y direction when using the Euler–Bernoulli beam element. The excitation in y direction would not cause any deformation in the x direction.

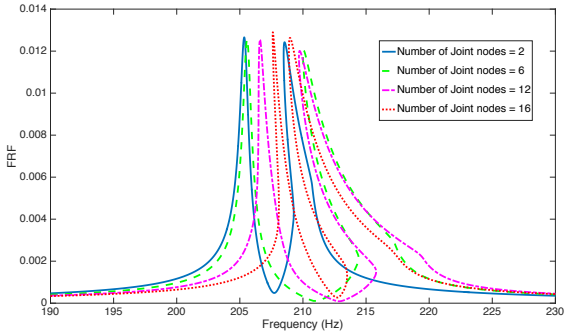

Figure 11 Forced frequency response close to the 2nd normal mode pair with the increasing number of interface nodes

ROM SENSITIVITY ANALYSIS

Figure 12 shows an example of the forced frequency response evaluated by using abovementioned seven ROM methods (with the excitation level of 5N, joint nodes number of 12 and mode number of 5 for each substructure). The result shows all of the ROM methods can capture well the global variations of the frequency response curve of the full solution. However, one can observe the differences between ROM methods when zooming in the peak response close to the out-of-phase mode. It is worth noting that the evaluated frequency points between ROM methods are not consistent due to the adaptive step algorithm in the continuation technique. In order to make direct comparisons possible, a cubic interpolation process is used. In this way, the relative error of these ROM methods at a particular frequency range can be computed. A sensitivity study is then performed to investigate the effect of the excitation level, size of interface nodes and also the number of normal modes on the performance of these ROMs.

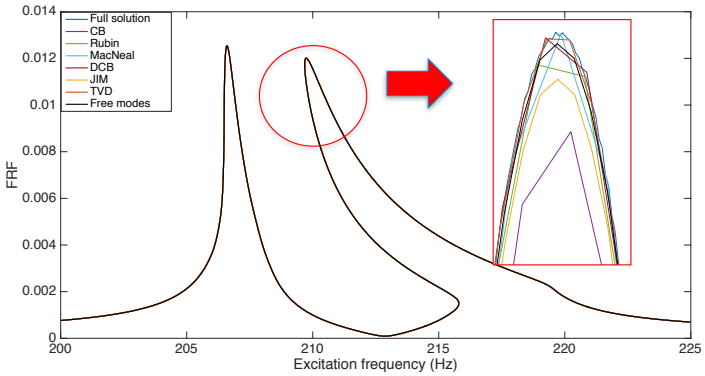

Figure 12 An example of the forced frequency response using different types of ROMs (CB, Rubin, MacNeal, DCB, JIM, TVD and free interface modes)

EXCITATIONAL LEVEL

Figure 13 shows relative FRF errors of various ROM methods with the increase of excitation level at 0.1N, 1N, 5N and 10N (5 modes for each substructure and 6 interface nodes). Please note that the number of frequency point is used as the title for x axis rather than the frequency because each excitation frequency might contain more than one response points. Each frequency point represents a unique response point at a particular frequency. The frequency point of out-of-phase resonance peak is remarked by black dash line. Figure 14 and 15 are plotted in the same way.

Figure 13 shows, with the increase of the excitation force, the relative error of Rubin, MacNeal and CB methods gradually go up. TVD, DCB, free interface methods stay in the similar errors. Consistent with the linear case, the CB method still results in largest relative error in the resonance response peak among all other methods, which becomes more significant when the excitation level increases. TVD, Rubin and MacNeal turn out the most accurate ones. However, Rubin and MacNeal methods are not very robust comparing to the TVD ones. The relative error of Rubin and MacNeal fluctuate quite a lot with the increase of excitation levels. One can see that their errors at the excitation level of 5 N become much larger than the TVD method.

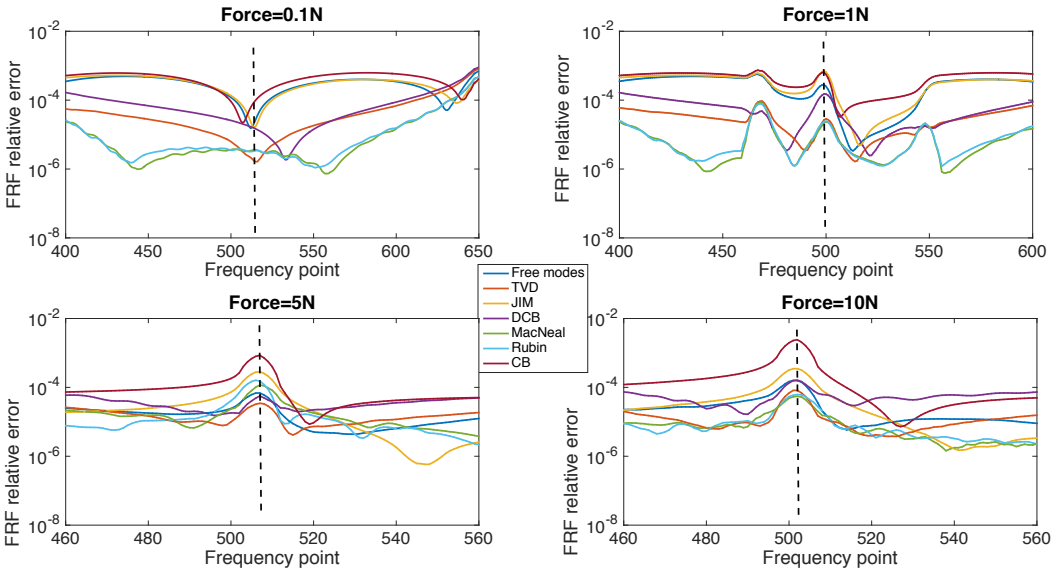

Figure 13 Relative FRF errors of various ROM methods with the different excitation levels in the region of out-of-phase mode

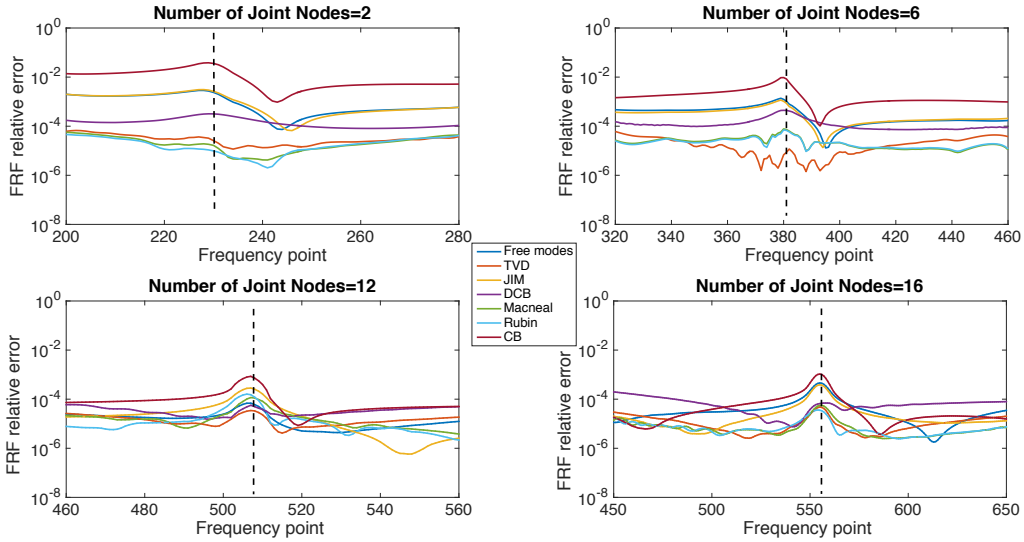

Figure 14 Relative FRF errors of various ROM methods with the different size of the contact interface in the region of out-of-phase mode

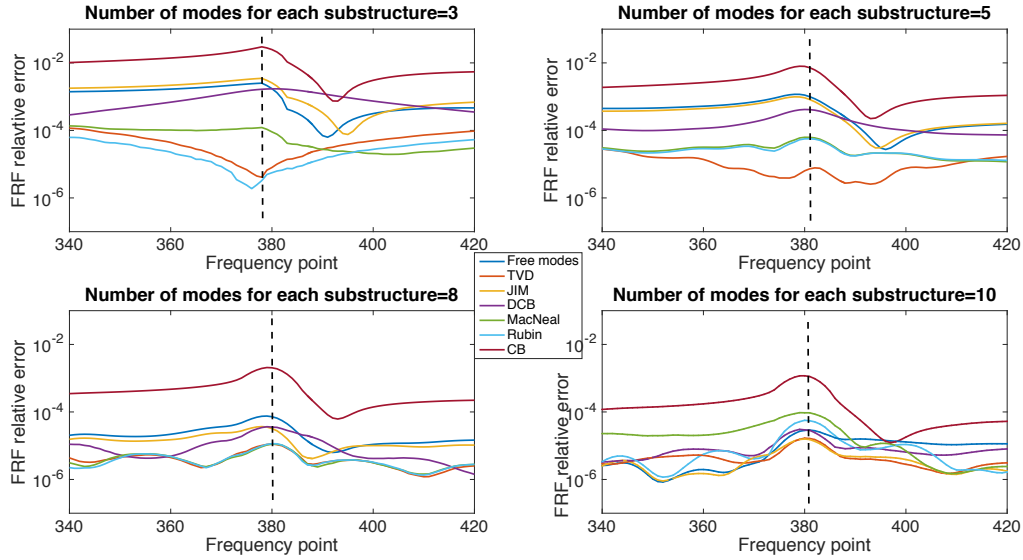

Figure 15 Relative FRF errors of various ROM methods with the increasing mode number in the region of out-of-phase mode

THE NUMBER OF JOINT NODES

Figure 14 shows the relative errors of all the ROM methods with different interface configurations in the frequency region of the out-of-phase mode (with the excitation level of 5 N and 5 normal modes for each substructure). In general, the average error of CB, JIM and free interface methods decreases when joint interface size increases. DCB, Rubin, MacNeal and TVD methods maintain similar relative error levels between 10^{-4} and 10^{-5}. The error curve of Rubin and MacNeal methods always stick together but their relative errors fluctuate a lot with size of the joint interface. JIM method results in much lower relative errors than the free interface modes method. Overall, TVD method is the most accurate and robust one with the increasing size of contact interface.

THE NUMBER OF MODES

Figure 15 shows the relative FRF errors of different ROM methods with the different number of normal modes (at excitation level of 5N and number of joint nodes of 6). The result shows that Rubin and TVD methods converge to 10^{-5} using only 3 modes for each substructure. However, with the increase of the mode number, the accuracy of the Rubin method unexpectedly rolls back in the case of mode number 5; it then comes back to the level of the TVD method at mode number 8 and then goes back again. It indicates the Rubin method are not very robust with increase of normal modes. In contrast, CB, DCB and free interface methods have monotonic convergence rate when the number of modes goes up. JIM can also reach the same accuracy as Rubin method at the mode number of 10.

CONCLUSION

The objective of this paper was to assess the capability of the classic CMS and recently developed ROM techniques for simulating the dynamics of jointed structures with contact nonlinearities. A 2D jointed beam with a linear and nonlinear joint has been considered as two test cases. Seven states of the art ROM methods have been selected for such a numerical assessment. For linear case, the relative errors of NF, MAC are compared between these ROM techniques. Rubin method outperforms the other methods in term of NF and MAC errors but experiences some numerical instability in the low frequency region when the size of the interface node increases. In terms of accuracy, TVD method achieves the second best. It is also the most computational efficient one having the smallest reduction ratio. The resulting reduced model using such a method can be independent of the joint interface size. The reduced order models using JIM and DCB method have the same reduction ratio and also they result in the similar accuracy to TVD method from the fourth mode. The reformulated DCB method has better performance on the low modes when the interface nodes number increase. The linear case also shows that the MacNeal method is not suitable for a jointed structure with a large joint interface, which may lead to the unacceptable errors. For nonlinear test, a 2D macro-slip contact friction model with stuck, slip and gap states were employed. The FRF of this nonlinear jointed structure was obtained by using a MHB method with AFT techniques. A sensitivity study was performed to investigate the effect of the excitation levels, the size of joint interface nodes and the number of normal modes on the dynamics of this assembled structure. In consistent with the linear case, Rubin method still achieves the lowest relative FRF errors among all the ROM methods. For this particular low order model, TVD method not only can achieve similar accuracy to Rubin methods but also more robust when the number of interface nodes and normal modes increases. The CB method still results in largest errors for both linear and nonlinear cases when comparing to the rest of methods. The relative error of this method increases when the nonlinearities of the system become strong. However, compared to free interface methods like the Rubin method, the CB method appears more numerically stable and robust. JIM method has not shown the obvious advantage compared to the free interface method. It might be due to the weak elastic coupling between nodes in the joint and inner structures that needs further investigations in future.

ACKNOWLEDGMENTS

The authors would like to acknowledge the support of Rolls-Royce plc for this research through the Vibration University Technology Centre (UTC) at the Imperial College London, UK. Special acknowledgement goes also to GEMinIDS project (WP3.3) jointly supported by Innovate UK and Rolls-Royce plc (http://gtr.rcuk.ac.uk/projects?ref=113088)

isaac.be/downloads/isma2016/papers/isma2016_0195.pdf

REFERENCES

[1] M.R.W. Brake, J. Groß, R.M. Lacayo, L. Salles, C.W. Schwingshackl, P. Reuß, J. Armand, Reduced Order Modeling of Nonlinear Structures with Frictional Interfaces, in: M.R.W. Brake (Ed.) The Mechanics of Jointed Structures: Recent Research and Open Challenges for Developing Predictive Models for Structural Dynamics, Springer International Publishing, 2018, pp. 427-450. https://doi.org/10.1007/978-3-319-56818-8_24

[2] R.A. Ibrahim, C.L. Pettit, Uncertainties and dynamic problems of bolted joints and other fasteners, Journal of sound and Vibration, 279 (2005) 857-936.https://doi.org/10.1016/j.jsv.2003.11.064

[3] H. Goyder, D. Lancereau, P. Ind, D. Brown, Friction and damping associated with bolted joints: results and signal processing, ISMA, Leuven, Belgium, 2016, http://past.isma-

[4] M. Krack, L. Panning-von Scheidt, Nonlinear Modal Analysis and Modal Reduction of Jointed Structures, The Mechanics of Jointed Structures, Springer, 2018, pp. 525-538.https://doi.org/10.1007/978-3-319-56818-8_29

[5] C.F. Beards, Damping in structural joints, Shock and Vibration Information Center The Shock and Vibration Digest, 14 (1982) 9-11.https://doi.org/10.1177/058310247901100904

[6] E.P. Petrov, D.J. Ewins, Effects of damping and varying contact area at blade-disk joints in forced response analysis of bladed disk assemblies, Journal of Turbomachinery, 128 (2006) 403-410.https://doi.org/10.1115/1.2181998

[7] E.P. Petrov, A high-accuracy model reduction for analysis of nonlinear vibrations in structures with contact interfaces,

Journal of Engineering for Gas Turbines and Power, 133 (2011) 102503 http://doi.org/10.1115/1.4002810
[8] M. Krack, L. Salles, F. Thouverez, Vibration Prediction of Bladed Disks Coupled by Friction Joints, Archives of Computational Methods in Engineering, 24 (2017) 589-636. https://doi.org/10.1007/s11831-016-9183-2
[9] J. Yuan, F. Scarpa, G. Allegri, B. Titurus, S. Patsias, R. Rajasekaran, Efficient computational techniques for mistuning analysis of bladed discs: A review, Mechanical Systems and Signal Processing (2016).https://doi.org/10.1016/j.ymssp.2016.09.041
[10] S. Huang, Dynamic analysis of assembled structures with nonlinearity, Department of Mechanical Engineering, Imperial College London, 2008, http://www.imperial.ac.uk/media/imperial-college/research-centres-and-groups/dynamics/40055709.PDF
[11] S. Zucca, B.I. Epureanu, Bi-linear reduced-order models of structures with friction intermittent contacts, Nonlinear Dynamics, 77 (2014) 1055-1067.https://doi.org/10.1007/s11071-014-1363-8
[12] F. Pichler, W. Witteveen, P. Fischer, Reduced-Order Modeling of Preloaded Bolted Structures in Multibody Systems by the Use of Trial Vector Derivatives, Journal of Computational and Nonlinear Dynamics, 12 (2017) 051032.http://doi.org/10.1115/1.4036989
[13] J. Armand, L. Pesaresi, L. Salles, C.W. Schwingshackl, A Multiscale Approach for Nonlinear Dynamic Response Predictions With Fretting Wear, Journal of Engineering for Gas Turbines and Power, 139 (2017) 022505.http://doi.org/10.1115/1.4034344
[14] R. Gasch, K.X. Knothe, Strukturdynamik: Bd. 2. Kontinua und ihre Diskretisierung, Springer, 1989http://www.springer.com/gp/book/9783540507710
[15] J. Becker, L. Gaul, CMS methods for efficient damping prediction for structures with friction, Proceedings of the IMAC-XXVI, Orlando, (2008) http://www.imperial.ac.uk/media/imperial-college/research-centres-and-groups/dynamics/becker_gaul.pdf
[16] W. Witteveen, H. Irschik, Efficient mode-based computational approach for jointed structures: joint interface modes, AIAA Journal, 47 (2009) 252.https://doi.org/10.2514/1.38436
[17] W. Witteveen, F. Pichler, Efficient model order reduction for the dynamics of nonlinear multilayer sheet structures with trial vector derivatives, Shock and Vibration, (2014), article ID 913136.http://dx.doi.org/10.1155/2014/913136
[18] D.J. Segalman, Model reduction of systems with localized nonlinearities, Journal of Computational and Nonlinear Dynamics, 2 (2007) 249-266.http://doi.org/10.2172/886648
[19] S. Jain, Model Order Reduction for Non-Linear Structural Dynamics, (2015), Master Thesis https://repository.tudelft.nl/islandora/object/uuid%3Acb1d7058-2cfa-439a-bb2f-22a6b0e5bb2a
[20] L. Pesaresi, L. Salles, A. Jones, J.S. Green, C.W. Schwingshackl, Modelling the nonlinear behaviour of an underplatform damper test rig for turbine applications, Mechanical Systems and Signal Processing, 85 (2017) 662-679.https://doi.org/10.1016/j.ymssp.2016.09.007
[21] F.M. Gruber, D.J. Rixen, Evaluation of substructure reduction techniques with fixed and free interfaces, Strojniški vestnik-Journal of Mechanical Engineering, 62 (2016) 452-462 http://dx.doi.org/10.5545/sv-jme.2016.3735
[22] S. Bograd, P. Reuss, A. Schmidt, L. Gaul, M. Mayer, Modeling the dynamics of mechanical joints, Mechanical Systems and Signal Processing, 25 (2011) 2801-2826 https://doi.org/10.1016/j.ymssp.2011.01.010
[23] E.P. Petrov, D.J. Ewins, Analytical formulation of friction interface elements for analysis of nonlinear multi-harmonic vibrations of bladed discs, Journal of Turbomachinery, 2002, pp. 899-908.http://doi.org/10.1115/1.1539868
[24] L. Salles, L. Blanc, F. Thouverez, A.M. Gouskov, P. Jean, Dynamic analysis of a bladed disk with friction and fretting-wear in blade attachments, ASME Turbo Expo 2009, 2009, pp. 8-12.http://doi.org/10.1115/GT2009-60151
[25] T.M. Cameron, J.H. Griffin, An alternating frequency/time domain method for calculating the steady-state response of nonlinear dynamic systems, Journal of applied mechanics, 56 (1989) 149-154.http://doi.org/10.1115/1.3176036
[26] R. Seydel, Practical bifurcation and stability analysis, Springer Science & Business Media, 2009.https://doi.org/10.1007/978-1-4419-1740-9
[27] S. Nacivet, C. Pierre, F. Thouverez, L. Jezequel, A dynamic Lagrangian frequency–time method for the vibration of dry-friction-damped systems, Journal of Sound and Vibration, 265 (2003) 201-219.https://doi.org/10.1016/S0022-460X(02)01447-5
[28] E. Sarrouy, J.-J. Sinou, Non-linear periodic and quasi-periodic vibrations in mechanical systems-on the use of the harmonic balance methods, Advances in Vibration Analysis Research, InTech, 2011.http://doi.org/10.5772/15638
[29] M. Pastor, M. Binda, T. Harčarik, Modal assurance criterion, Procedia Engineering, 48 (2012) 543-548.https://doi.org/10.1016/j.proeng.2012.09.551